

High-speed 3D shape measurement with structured light methods: A review

Song Zhang

School of Mechanical Engineering, Purdue University, West Lafayette, IN 47907, USA



ARTICLE INFO

Keywords:

High speed
3D Shape measurement
3D Imaging
Structured light
High accuracy

ABSTRACT

High-speed 3D shape measurement (or imaging) has seen tremendous growths over the past decades, especially the past few years due to the improved speed of computing devices and reduced costs of hardware components. 3D shape measurement technologies have started penetrating more into our daily lives than ever before with the recent release of iPhone X that has an built-in 3D sensor for Face ID, along with prior commercial success of inexpensive commercial sensors (e.g., Microsoft Kinect). This paper overviews the primary state-of-the-art 3D shape measurement techniques based on structured light methods, especially those that could achieve high measurement speed and accuracy. The fundamental principles behind those technologies will be elucidated, experimental results will be presented to demonstrate capabilities and/or limitations for those popular techniques, and finally present our perspectives on those remaining challenges to be conquered to make advanced 3D shape measurement techniques ubiquitous.

© 2018 Elsevier Ltd. All rights reserved.

1. Introduction

With recent advancements on personal computers, mobile devices, and cloud computing, high-speed and high-accuracy 3D shape measurement (or imaging) techniques have been increasingly sought by scientists in fields such as biomedical engineering and computer science, by engineers from various industries including the manufacturing and entertainment, and even by ordinary people with different technical backgrounds. The commercial success of consumer level real-time 3D imaging technologies including Microsoft Kinect, Intel RealSense, and recently Apple iPhone X propels the application developments and simultaneously drives the needs for better 3D imaging technologies.

High-speed 3D imaging technologies can be classified into two major categories: the passive and the active methods. The passive techniques use no active illumination for 3D reconstruction with stereo vision [1,2] being one of the most popular methods. The stereo-vision system captures images from at least two different perspectives, and analyzes the images to find corresponding points from those images for 3D coordinate calculation based on triangulation. The stereo vision method is very simple since only cameras are used, and can also be very fast, as fast as the camera can capture images. Hinging on detecting the corresponding pairs from different images, the measurement accuracy of this method varies depending upon the object to be measured, and could be very low if an object does not present rich surface texture. Furthermore, it is difficult for such a technique to achieve camera pixel spatial resolution due to the use of various image correlation methods for stereo correspondence determination.

The active methods, in contrast, actively illuminate the object to facilitate 3D reconstruction. As one of the extensively adopted active methods, the time-of-flight (TOF) technique uses an active emitter to modulate the light in time domain, an optical sensor collects the light scattered back by the object, recovers depth information by calculating the time delay from the signal leaves the device and the signal returns to the device [3]. Unlike the stereo-vision method, the TOF method does not require triangulation for 3D reconstruction, and thus the entire system can be very compact, making it applicable for mobile applications. However, because light travels very quickly, the achievable depth resolution is typically not high for short range measurement. Kinect II employs the TOF technique for real-time 3D imaging, and successfully finds its applications in human computer interaction where neither accuracy or spatial resolution requirement is high.

The structured light technique belongs to one of the active methods and utilizes a projection device to actively project structured patterns. The structured light system is similar to a stereo system with the difference of replacing one camera with a projector. The projected structured patterns carry encoded information to resolve the fundamentally difficult correspondence problem of the stereo vision technique. Numerous codification methods have been developed with some being discussed by Salvi et al. [4]. Due to the flexibility and versatility of structured light methods, 3D shape measurement using structured light methods has been a vibrant field with increased interest in development and employment. In particular, high-speed and high-accuracy 3D shape measurement techniques become more and more important with new applications found almost every day. Therefore, this paper will primarily

E-mail address: szhang15@purdue.edu

<https://doi.org/10.1016/j.optlaseng.2018.02.017>

Received 16 December 2017; Received in revised form 21 February 2018; Accepted 23 February 2018

Available online 13 March 2018

0143-8166/© 2018 Elsevier Ltd. All rights reserved.

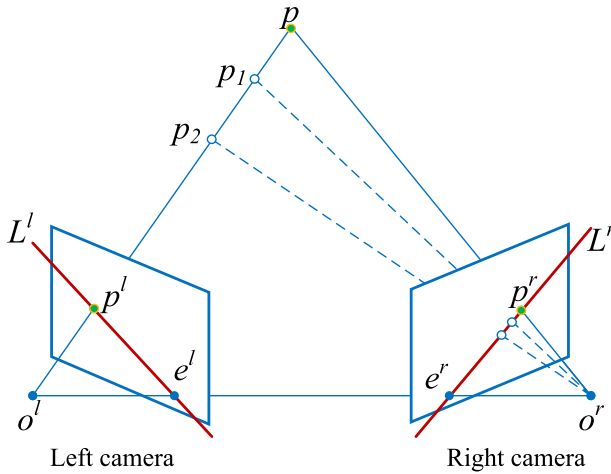


Fig. 1. Epipolar geometry for a standard stereo vision system.

focus on structured light methods that could achieve high measurement speed and high measurement accuracy. Specifically, this paper elucidates the principles of various coding methods, discusses their advantages or shortcomings, and presents some experimental data obtained by structured light methods.

It should be noted that, due to our limited knowledge and the page constraints, this paper, by no means, intends to elaborate all state-of-the-art 3D shape measurement/imaging technologies, albeit we endeavor to cover as many as existing techniques as possible. The readers are encouraged to refer to some other review papers on 3D shape measurements such as [5–10].

The paper is organized as follows: Section 2 presents the basics of structured light technique including system calibration. Section 3 introduces relevant principles of structure encoding methods along with some experimental results to demonstrate their performances; Section 4 discusses our perspectives on the challenges in this field; and Section 5 summarizes this paper.

2. Basics of structured light techniques

This section briefly explains the basic principles behind structured light techniques that use triangulation for 3D reconstruction, the epipolar geometry that could simplify structured pattern design strategies, and then the calibration methods that estimate physical properties of the structured light system.

2.1. Basics of epipolar geometry

Structured light techniques originated from the conventional stereo vision method that recovers 3D information by imitating human perception system. The stereo-vision system captures two images from different perspectives, as illustrated in Fig. 1. For a given point p in a 3D space, p^l and p^r are the imaging points on two 2D imaging planes. If the corresponding pair (i.e., p^l and p^r) can be found by analyzing those two images, (x, y, z) coordinates of point p can be calculated using triangulation assuming the optical parameters (e.g., focal length for camera lens, principal point) and geometric parameters (e.g., transformation from one camera to the other) are known. The parameters required for 3D reconstructions can be calibrated, which will be detailed in Section 2.3. In computer vision, *epipolar geometry* is developed to increase the robustness and simplify the correspondence determination [11,12]. Epipolar geometry essentially constrains the stereo searching by using the geometric constraints of the stereo vision system. The focal points of the lenses o' and o'' and the object point p forms a plane called *epipolar plane*, and the intersection between the epipolar plane and a imaging plane is a line that is called *epipolar line*. L^l and L^r shown on Fig. 1 is the

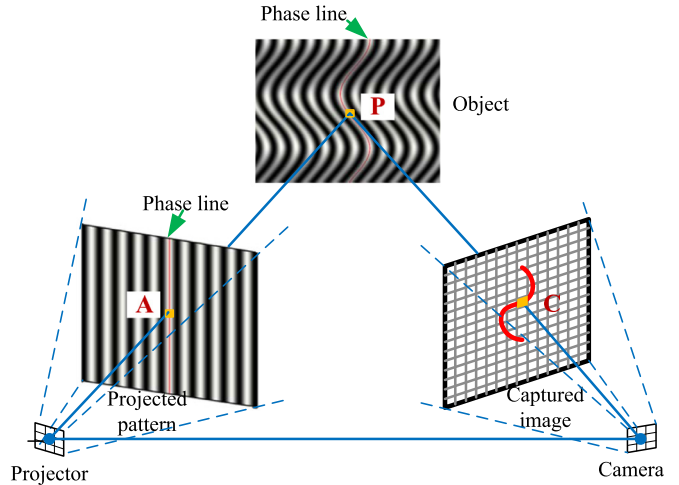


Fig. 2. Schematic diagram of a typical structured light system.

epipolar line on left and right camera image, respectively. Since the true corresponding point pairs must lie on the epipolar line, the original 2D corresponding searching problem becomes 1D, making it more efficient and robust. The intersection point between the line $o'o''$ and the camera image plane is called epipole. e^l and e^r , shown in Fig. 1, is the epipole for the left and right camera, respectively. For a given point on the left camera p^l , the epipolar plane can be formed by combining the point p^l with two other known points, the focal point o' and the epipole e^l , and thus the epipolar lines L^l and L^r can be mathematically calculated once the system is calibrated.

To further improve the correspondence searching speed, stereo images are rectified such that the corresponding point only occurs on the same row; and the process of rectifying stereo images is often referred as *image rectification*. Image rectification essentially translates and rotates the original images to align those epipolar lines (e.g., make L^l and L^r on the same line) using the stereo-vision system calibration data. Numerous global or semi-global stereo-matching algorithms [13–19] have developed to find the corresponding points using the epipolar geometry with some optimization strategies. The stereo-matching algorithm typically generates a disparity map that stores the pixel shift of a corresponding pairs from the left camera image to the right camera image. The disparity map is then used to reconstruct (x, y, z) coordinates for each point based on the calibrated system parameters. Since only two cameras are used, the stereo-vision technique has obvious advantages: the simplicity of hardware configuration and straightforward calibration for the system [20]. However, heavily relying on natural texture for correspondence establishments, the accuracy of stereo-vision techniques varies from one object to another; and the measurement accuracy is not high if an object has no obvious distinctive features.

2.2. Basics of structured light technique

The structured light technique fundamentally eliminates the stereo-vision problem by replacing one of the cameras of the stereo-vision system with a projector and actively projecting known feature points [4]. Fig. 2 shows the schematic diagram of a 3D shape measurement system based on one type of structured light technique. The projector shines structured patterns onto the object whose geometry distorts structured patterns. A camera captures the distorted structured images from another perspective. In such a system, the correspondence is established by analyzing the distortion of captured structured images with known features (e.g., phase line) projected by the projector. Once the system is calibrated and the correspondence is known, (x, y, z) coordinates can be reconstructed, using a method similar to that used by stereo vision techniques.

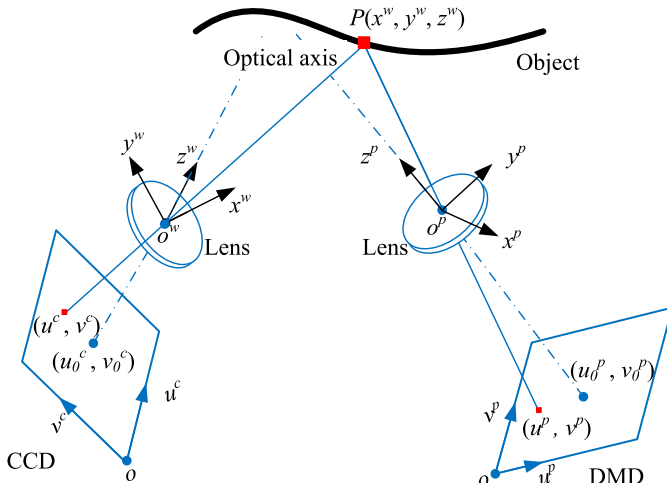


Fig. 3. Pinhole model for stereo system with the world coordinate system coinciding with the camera lens coordinate system.

2.3. Structured light system calibration

Accurate system calibration, which usually involves complicated and time consuming procedures, is crucial for any 3D shape measurement systems. The structured light system calibration essentially determines the relationship between a point in the world coordinates and that on the camera or project image plane coordinates. Though not highly accurate for large depth range measurement, the simple reference-plane-based methods [21–24] are extensively adopted, especially in interferometry systems, mainly because of their simplicity.

More accurate methods involve the calibrations of camera, projector, and geometric relationship between these two devices for a single projector and singe camera structured light system. Typically, the camera is described as a pinhole model [25], as illustrated in Fig. 3. The pinhole model mathematically describes the transformation from the world coordinate system (x^w, y^w, z^w) to the camera lens coordinate system (x^c, y^c, z^c) and the projection from the lens coordinate system to the image coordinate system (u^c, v^c) as

$$[u^c, v^c, 1]^T = \mathbf{A} \cdot [\mathbf{R}, \mathbf{t}] \cdot [x^w, y^w, z^w, 1]^T, \quad (1)$$

where T denotes matrix transpose, \mathbf{A} is a 3×3 intrinsic matrix that represents the focal length and the principle point of the imaging system, \mathbf{R} is a 3×3 rotation matrix and \mathbf{t} is a 3×1 translation vector. The transformation matrix $[\mathbf{R}, \mathbf{t}]$ represents the *extrinsic parameters* that describes the transformation from the world coordinate system to the camera lens coordinate system, and \mathbf{A} represents the *intrinsic parameters* that describes the projection from 3D lens coordinates to 2D image coordinates. Camera calibration essentially estimates the intrinsic and extrinsic parameters with numerous methods [26–28] being developed and documented including open source codes (e.g., OpenCV calibration toolbox) for practical use. One of the most popular camera calibration method was developed by Zhang [25] that only requires a flat calibration plane with some known feature points on the plane (e.g., checkerboard, circle patterns).

Although numerous methods have been developed for structured light system calibration [29–35], they are conventionally difficult and complex because the projector cannot freely capture images like a camera. Zhang and Huang [36] developed a method that is now extensively adopted in both academia and industry. Such a method enables the projector *capture* images like a camera, and thus the complicated projector calibration problem becomes a well-established camera calibration problem, and the structured light system calibration follows the same calibration procedure used by a standard stereo-vision system. All existing calibration methods work well under the assumption that both the projector and the camera are nearly focused. To relax such strong con-

straints and further simplify structured light system calibration, Li et al. [37] developed a method for out-of-focus projector calibration by allowing a projector only “capture” the center point of a pixel such that the problem caused by defocusing (i.e., image blurring) can be completely eliminated; Bell et al. [38] developed a method that enabled the out-of-focus camera calibration by encoding the calibration feature points in an active calibration target; and the intrinsic and extrinsic parameter calibration separation method developed by An et al. [39] made structured light even more flexible.

3. Structure light codification methods

This section elucidates some major codification strategies that could be used for high-speed 3D shape measurement with some being commercially available. In particular, we will discuss various structured pattern construction methods that lead to various high-speed applications, and present experimental data to illustrate the principles or demonstrate the potentials of some representative high-speed 3D shape measurement techniques.

3.1. Statistical pattern

As discussed in Section 2.2, the ultimate goal of any structured light technology is to project some known structured patterns such that the one-to-one correspondence between a projector point and a camera point can be robustly established. One of the simplest approach is to encode locally unique features onto the structured pattern such that for any given point on the camera image (u^c, v^c) , the corresponding projector point can be uniquely determined. Typically, a kernel of $w_m \times w_n$ pixels is unique within the entire projected image. The statistically random coding method has been successfully employed on consumer products (e.g., Microsoft Kinect V1, Intel RealSense R200, iPhone X). Fig. 4 shows the statistically random pattern that is used by Kinect I, RealSense, and iPhone X. Clearly the projected patterns are all random in nature, albeit their distribution are different.

The merits of this encoding method are:

- *Easy to understand.* This is a straightforward method to address the limitation of stereo matching method where the corresponding projector for a given camera pixel can be uniquely located by analyzing the statistical pattern. 3D reconstruction is also straightforward based on triangulation.
- *Easy to implement.* Since only a single static pattern is required, it is easy to implement such method on a digital video projector, a laser speckle projector, and even a slider projector.
- *Easy to miniaturize.* The static pattern can be easily realized by a simple hardware and thus the miniaturization difficulty level is not high. This is one of the major reasons that such a method is adopted in inexpensive commercial 3D sensors (e.g., Kinect V1 and iPhone X).

However, this method has the following fundamental limitations:

- *Spatial resolution is low.* The spatial resolution is constrained by the pattern generator in both u and v direction, and the achievable spatial resolution is also much lower than the camera resolution because the encoded features must be distinguishable from camera images (e.g., each feature must be large than one camera pixel).
- *Sensitivity to noise is high.* The background light is directly blended with the projected light to be imaged by the camera, and the capture combined intensity image is used for correspondence determination. Therefore, when the background lighting is strong, the signal-to-noise ratio (SNR) is low, and thus determining the corresponding point becomes difficult.
- *Measurement accuracy is low.* It is difficult for this method to achieve projector and camera pixel level correspondence accuracy because

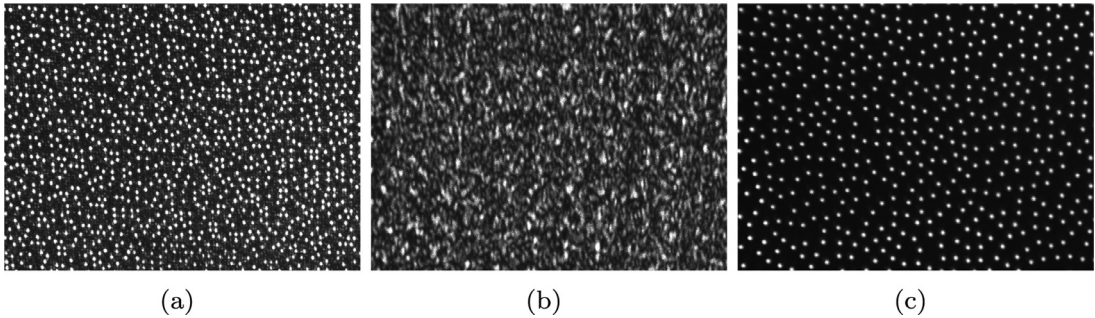


Fig. 4. Random patterns projected by the commercial 3D sensors. (a) Microsoft Kinect V1; (b) Intel RealSense R200; (c) Apple iPhone X.

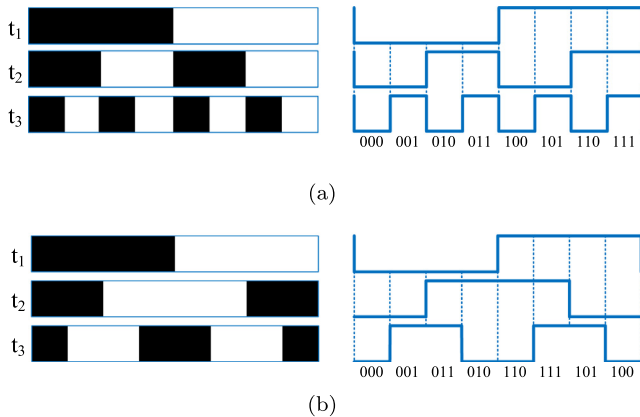


Fig. 5. Representative binary coding methods. (a) Simple binary coding; (b) gray coding.

the correlation method requires windowed many pixels to statistically determine the most possible matching point instead of mathematically precisely defined point. Due to the low correspondence determination accuracy, it is difficult for such a method to achieve high measurement accuracy.

3.2. Binary coding

To address some of the limitations of the statistical pattern based method, binary coding methods were developed. As discussed in [Section 2.2](#), the epipolar geometry constraints reduce the 2D correspondence problem to be a 1D problem, and thus if u^p or v^p coordinate (NOT both) is uniquely determined for a given camera point (u^c, v^c) , 3D coordinates of the object can be determined. Instead of making the encoded pattern unique in both u and v direction, structured patterns only need to be unique in one direction (e.g., patterns with structured stripes). One of the most straightforward methods is to represent each stripe on the projector with a unique code (i.e. codeword) that can be realized by projecting a sequence of black or white patterns. Assume black represents 0 and white represents 1, the sequence of 0's and 1's can be captured by the camera and decode the corresponding stripe on the projector.

[Fig. 5](#) shows two representative coding methods to represent 8 unique stripes. The simple coded patterns are illustrated on the left of [Fig. 5a](#) and the corresponding binary coding is shown on the right. This coding method is straightforward because it simply represents 8 sequential integer numbers with the corresponding binary bits. If these three patterns shown on the left are projected sequentially at time t_1 , t_2 , and t_3 , the captured image can be binarized to decode the binary sequence shown on the right, the codeword for each camera pixel can be deter-

mined, and thus the unique correspondence can be established for those 8 stripes for 3D reconstruction. [Fig. 5b](#) shows another binary coding method called gray coding. Comparing with the simple coding method shown in [Fig. 5a](#), gray-coding only allows one of the sequence patterns to change its status (from 0 to 1 or from 1 to 0) at a given projector pixel, while simple coding does not have such a constraint. Due to sampling, the camera may not precisely capture the location of the transition pixels, and thus the simple coding is prone to more sampling errors than the gray coding method.

[Fig. 6](#) shows the comparing results using these two different coding methods. For each coding method, one single projector pixel is encoded with a different codeword, and thus the highest possible resolution that the projector can create. [Fig. 6b](#) shows the densest gray-coded pattern that is so dense that it is not clearly visible to the camera. After decoding the sequence patterns, 3D shape can be reconstructed, as shown in [Fig. 6e](#). Similarly, the simple coding method can also be employed to perform 3D shape measurement. [Fig. 6i](#) shows the result without filtering, depicting some artifacts on the reconstructed surface (i.e., spikes). These spikes can be removed by filtering, and [Fig. 6j](#) shows the result after removing spikes. [Fig. 7a](#) and [b](#) respectively shows the closeup view of [Fig. 6j](#) and [e](#). Even after spike removal, the random noise created by the simple coding method is significantly larger than that produced by the gray coding method,

To reach high-speed 3D shape measurement, the structured patterns must be switched rapidly, and captured in a short period of time. For example, Rusinkiewicz and Levoy developed a real-time 3D shape measurement system [40] using the stripe boundary code [41] that only requires four binary patterns for codification. Such a system achieved 15 Hz 3D data acquisition speed.

Spacetime stereo is another technique that has potential for high speed 3D shape measurement [42–44]. To resolve the correspondence problem, a projector is used to project a sequence of active patterns for assistance. In a short period of time, a number of structured patterns are projected and captured by the camera. The correspondences between two camera pixels are identified based on the actively projected structured patterns. By using the active structured patterns, stereo matching can be done rapidly, thus this technique has the potential to achieve real-time 3D shape measurement. However, this technique has some drawbacks, (1) for any measurement point, the projector and two cameras must be able to “see” it. Therefore, it only measures the overlapping regions of the three devices, which is much smaller than any of them; (2) because stereo matching is utilized, it is very difficult for this technique to reach pixel-level resolution.

The binary coding methods improve over the statistical coding method in that the structured patterns is continuous in one dimension, and thus the measurement resolution in one direction can be as high as the camera pixel spatial resolution. The major advantages of binary methods are: (1) they are simple since the coding and decoding algorithms are very simple, (2) they are fast because the processing algorithm is computationally inexpensive, (3) they are fast because the band-

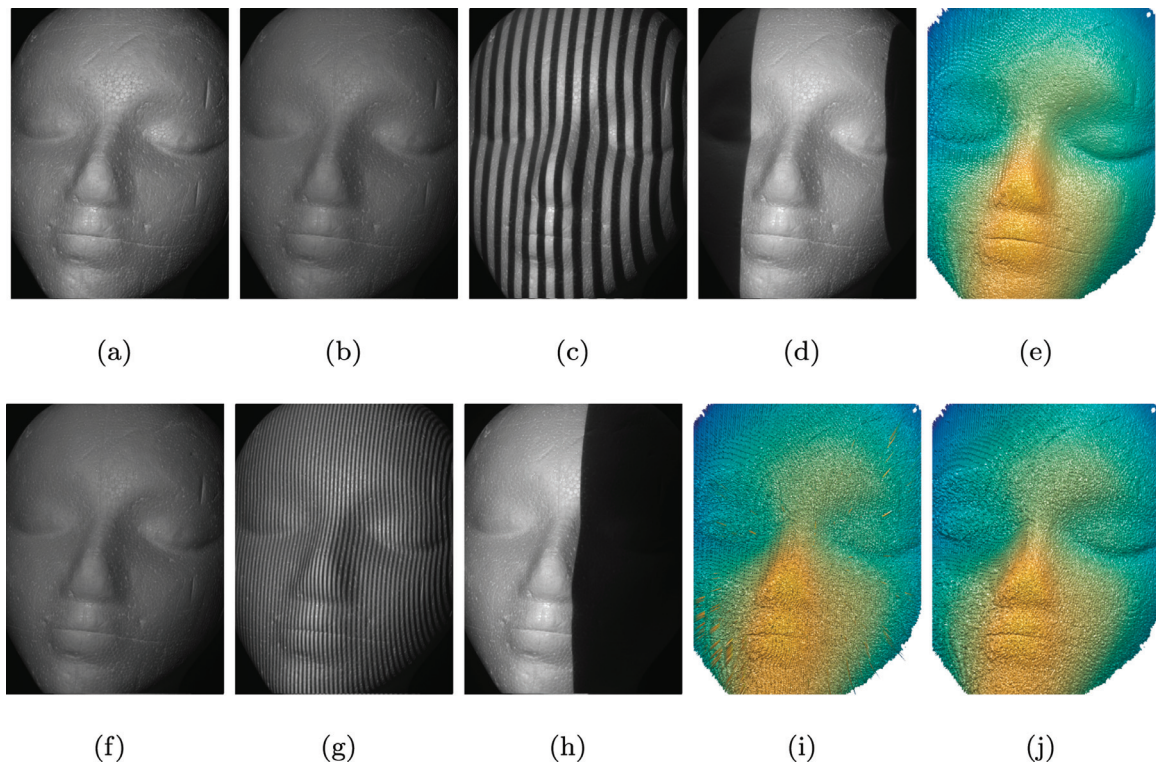


Fig. 6. Experimental results using two representative binary coding methods. (a) Photograph of the captured object; (b) densest gray coded pattern; (c) and (d) two representative gray coded patterns; (e) 3D reconstruction result without filtering using the sequence of gray coded patterns; (f) densest simple coded pattern; (g)-(h) two representative simple coded patterns; (i) 3D reconstruction result without filtering using the sequence of simple coded patterns; (j) 3D result after removing the spike noise shown in (i).

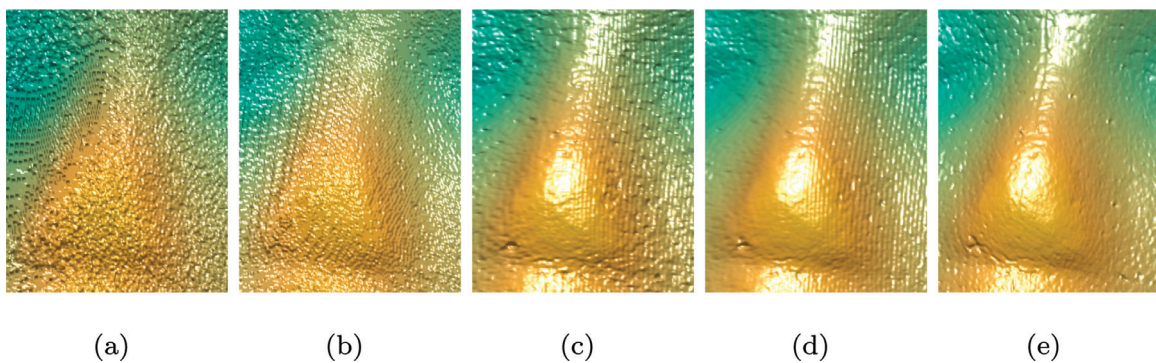


Fig. 7. Zoom-in views of 3D results reconstructed by different coding methods. (a) Zoom-in view of Fig. 6j; (b) Zoom-in view of Fig. 6e; (c) Zoom-in view of Fig. 8e; (d) Zoom-in view of Fig. 9e; (e) Zoom-in view of Fig. 11e.

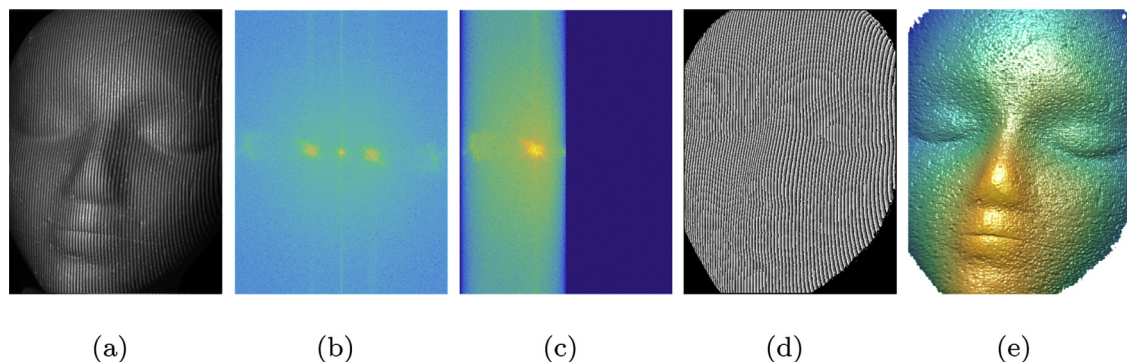


Fig. 8. 3D shape measurement using a single fringe pattern FTP method. (a) Fringe pattern; (b) frequency spectrum; (c) band-pass filtered frequency spectrum of (b); (d) wrapped phase; (e) recovered 3D shape.

width requirement of 1-bit binary pattern switching is low; and 4) they are typically robust since only two levels are required to be identified. However, the achievable spatial resolution across the binary stripes is fundamentally limited by both the projector pixel size and the camera pixel size, as demonstrated from the examples shown in Figs. 6 and 7.

3.3. Sinusoidal phase encoding

Though powerful and successful, the aforementioned statistical coding or binary coding methods are still limited by the projector's spatial resolution, and thus the matching accuracy is not high. Furthermore, all these methods are based on analyzing image intensity that is affected by surface texture, and thus the measurement accuracy could vary for object with different textures. Instead of determining the corresponding point in the intensity domain and discretely in at least one dimension, fringe analysis methods establish the correspondence in phase domain and continuous in both direction. Fringe analysis methods typically analyze sinusoidally varying structured patterns (called fringe patterns) to recover the phase of carrier fringe patterns. And the method of using a digital video projector to project desired sinusoidal fringe patterns for phase retrieval is called digital fringe projection (DFP) technique, albeit there are other means of generating sinusoidal fringe patterns such as coherent laser interference [45], white light interference [46], grating [47], Moiré [48], along with others.

Similarly, a single fringe pattern is sufficient to recover phase using Fourier transform [49], and 3D shape measurement techniques based on this method is often regarded as Fourier transform profilometry (FTP). Assume a sinusoidal fringe image can be represented as

$$I_1(x, y) = I'(x, y) + I''(x, y) \cos[\phi(x, y)], \quad (2)$$

where $I'(x, y)$ is the average intensity or the DC component, $I''(x, y)$ the intensity modulation, and $\phi(x, y)$ the phase to be solved for. This equation can be re-written in a complex form as

$$I_1(x, y) = I'(x, y) + 0.5 \cdot I''(x, y) [e^{j\phi(x, y)} + e^{-j\phi(x, y)}], \quad (3)$$

where $e^{j\phi(x, y)}$ is the conjugate of $e^{-j\phi(x, y)}$. The carrier signal $\tilde{I}(x, y)$ can be recovered by applying a band-pass filter in frequency domain to filter out the conjugate and DC component. The filtered image can be described as,

$$\tilde{I}_1(x, y) = 0.5 \cdot I''(x, y) e^{j\phi(x, y)}, \quad (4)$$

from which the phase can be solved for

$$\phi(x, y) = \tan^{-1} \left\{ \frac{\Im[\tilde{I}(x, y)]}{\Re[\tilde{I}(x, y)]} \right\}. \quad (5)$$

Here $\Im(\cdot)$ and $\Re(\cdot)$ respectively denotes the imagery and real part of a complex variable.

Applying a low-pass filter to Eq. (4) gives $I'(x, y)$ without fringe stripes, which can be used as texture or photograph of the object for rendering or additional information extraction.

The phase value obtained from Eq. (5) ranges from $[-\pi, +\pi]$ with a 2π modus due to the use of an arctangent function. The phase map obtained here is often regarded as *wrapped* phase map, and a continuous phase map is usually necessary for 3D shape reconstruction. The process to remove 2π discontinuities and generate continuous map is called phase unwrapping. Once the phase unwrapped, 3D shape for each pixel can be reconstructed by referring to a planar object, or using the geometrically calibrated parameters for coordinate calculations.

Conventionally, a spatial or temporal phase unwrapping algorithm can be adopted to unwrap the phase map. A spatial phase unwrapping algorithm (e.g., those discussed in [50] and [51]) analyzes the wrapped phase map itself and determines the number of 2π 's (or fringe order) to be added to a point based on surface smoothness assumption. The temporal phase unwrapping algorithm (e.g., [52–61]), in contrast, captures additional images to uniquely determines the fringe order uniquely for each pixel. The former works well for "smooth" geometry but could fail

if the surface has abrupt geometric changes or contains isolated patches. The latter can handle arbitrary surfaces, albeit it sacrifices measurement speeds.

Recently, researchers have developed methods to determine fringe order by using the inherent geometric constraints of a structured light system [62], or by adding a secondary camera to provide additional constraints for correct fringe order determination either through checking candidates backward forward [63–65] or applying a standard stereovision algorithm for fringe order initialization [66,67]. All these algorithms do not sacrifice data acquisition speed, but the geometric-constraint-based method has a limited depth range, adding a secondary camera increases the complexity and cost of the 3D shape measurement system.

Fig. 8 first row shows an example measurement using the FTP method. Fig. 8a shows the single fringe pattern captured by the camera, and Fig. 8b shows the corresponding frequency spectrum. This figure clearly shows that the DC component. After applying a band-pass filter, and Fig. 8c shows the spectrum after passing through a band-pass filter. Fig. 8d shows the wrapped phase map that is then unwrapped to reconstruct 3D shape shown in Fig. 8e.

Similar to a single statistical pattern based approach, the single-pattern FTP can achieve the highest possible data acquisition speeds (as fast as camera can capture). However, the conventional FTP methods have three major limitations: (1) they are sensitive to noise; (2) they have stringent requirements on surface optical properties (e.g., no strong texture); and (3) they have difficulty accurately measuring complex surface geometries. To alleviate the problems associated with FTP methods, Kemao [68,69] proposed Windowed Fourier Transform (WFT) method they have substantially increased the robustness [70] and broadly extended the applications [71] of FTP methods. Despite these advancements, single-pattern based Fourier transform method still cannot achieve high-measurement accuracy for complex surface geometry or objects with strong texture. This is because if the texture or geometry varies significantly across the surface, it would be challenging to separate the DC component and the carrier frequency.

To enhance the measurement capabilities of FTP method, Mao et al. [72] proposed a modified FTP method by adding a π -shifted pattern, $I_2(x, y)$,

$$I_2(x, y) = I'(x, y) + I''(x, y) \cos[\phi(x, y) + \pi], \quad (6)$$

taking the difference between $I_1(x, y)$ and $I_2(x, y)$ leads

$$I_d(x, y) = I_1(x, y) - I_2(x, y) = 2I''(x, y) \cos[\phi(x, y)]. \quad (7)$$

FTP method is applied to the difference pattern $I_d(x, y)$ without DC component.

Alternatively, Guo and Huang [73] proposed to directly project DC component, i.e., $I_2(x, y) = I'(x, y)$, and use the same fringe analysis method as Mao et al. [72] proposed. Since the DC component is fundamentally eliminated for these methods, the modified FTP methods substantially improve measurement quality and can, to some extent, tolerate surface texture.

Fig. 9 first row shows the example measurement using the modified FTP method. Fig. 9a shows the second fringe pattern $I_2(x, y)$, and Fig. 9b shows the frequency spectrum of the difference fringe pattern $I_d(x, y)$ without the DC component. The wrapped phase and corresponding 3D reconstructed result is shown in Fig. 9d and e, respectively. Comparing with the results shown in Fig. 8, the modified FTP method generates much high quality data. However, the modified FTP method requires two fringe patterns for 3D shape measurement, slowing down the measurement speed.

Due to high measurement speed, FTP methods have been demonstrated successful for fast motion capture applications, such as measuring vibration [74] or a flapping wing robot [75]. Su and Zhang [9] thoroughly reviewed the applications that the FTP method can be applicable, Zhang [7] compared different processing algorithms, and Takeda [8] summarized the extreme phenomena that the FTP method can be

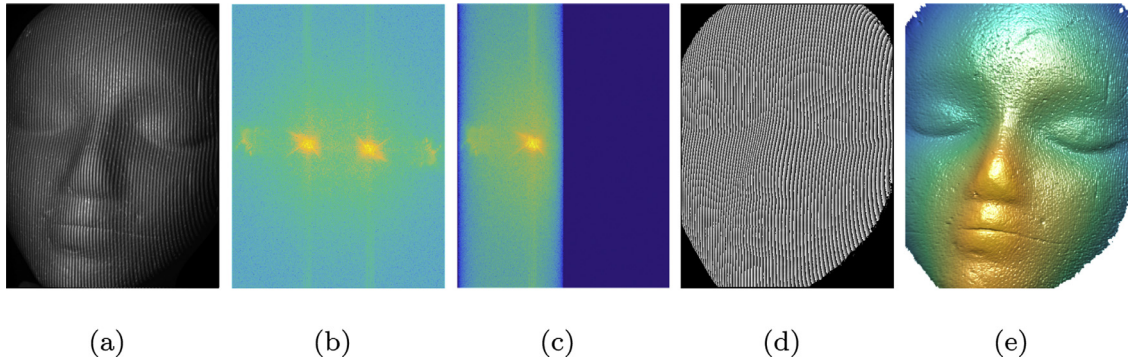


Fig. 9. 3D shape measurement using the modified FTP method. (a) Additional fringe pattern $I_2(x, y)$; (b) frequency spectrum of $I_d(x, y)$; (c) band-pass filtered frequency spectrum of (b); (d) wrapped phase; (e) recovered 3D shape.

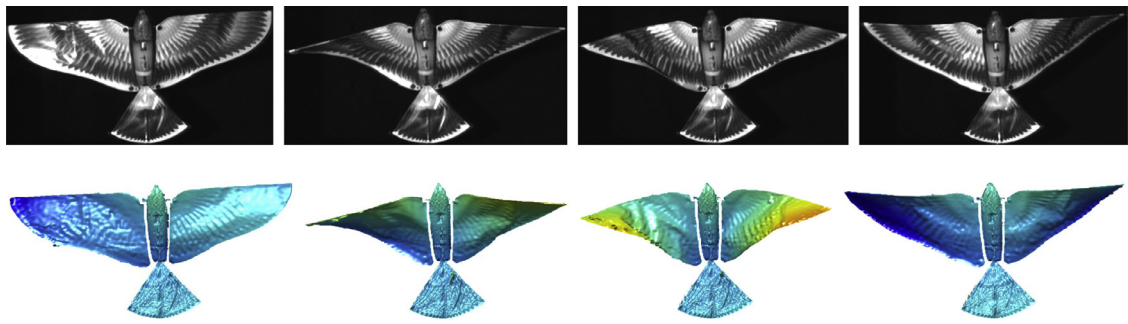


Fig. 10. High-speed 3D shape measurement results of rapidly flapping robotic wings (21 Hz) with a modified FTP method. The first row shows the photograph of the robot wing and the bottom row shows the corresponding 3D measurement results.

used to measure. Fig. 10 shows the measurement results of a flapping wing robot whose wings flap at 21 Hz, and the camera captured fringe patterns at 5 kHz. The results were originally published by Li and Zhang [75].

In general, the FTP or modified FTP method typically requires object surface to be smooth geometrically and without strong texture. This is because to properly recover carrier phase information, FTP requires the frequency of carrier sinusoidal signal to be much higher than the frequency signal introduced by surface geometry changes or texture. FTP methods, after all, extract phase for a point that either requires the knowledge of points locally or globally during the Fourier transform stage. Therefore, some limitations associated with FTP methods can be alleviated if the phase can be retrieved without using those neighborhood points. Since Eq. (2) has three unknowns $I(x, y)$, $I'(x, y)$, and $\phi(x, y)$, a minimum number of three equations is required to solve for the phase $\phi(x, y)$. Researchers have developed numerous phase shifting methods for pixel-by-pixel phase retrieval [76].

In general an N -step phase-shifting algorithm can recover the phase by

$$\phi(x, y) = -\tan^{-1} \left[\frac{\sum_{k=1}^N I_k(x, y) \sin(2\pi k/N)}{\sum_{k=1}^N I_k(x, y) \cos(2\pi k/N)} \right], \quad (8)$$

where

$$I_k(x, y) = I'(x, y) + I''(x, y) \cos[\phi(x, y) + 2\pi k/N]. \quad (9)$$

Typically, the larger the N is chosen, the higher the measurement accuracy can be achieved. For high speed applications, a three-step (i.e., $N = 3$) phase-shifting algorithm is used because the time required to capture required fringe images is shortest.

Fig. 11 shows the measurement result using a three-step phase-shifting algorithm (i.e., $N = 3$). From three phase-shifted fringe patterns shown in Fig. 11a–c, the wrapped phase can be computed. The wrapped phase can then be unwrapped for 3D reconstruction. Fig. 11d and e respectively shows the wrapped phase map and the corresponding 3D re-

sult. The measurement quality varies with the coding method employed. Fig. 7 shows the close-up views of those 3D reconstructions from different coding methods. Clearly both binary-coding methods produce lower quality data than the single pattern FTP method for a 3D object without strong texture, as shown in Fig. 7a–c. The double-pattern FTP method improves measurement quality, but the three-step phase-shifting algorithm generates the best quality data, although only one more pattern is used.

Furthermore, the three-step phase-shifting algorithm lands nicely on the digital video projection platform since these three fringe patterns can be encoded as three primary colors (red, green, blue or RGB). Leveraging the unique projection mechanism of the single-chip digital-light-processing (DLP) technologies, Zhang and Huang [77] developed probably the first-ever high-speed 3D shape measurement system using phase-shifting methods. The system achieved 3D shape acquisition, reconstruction and display at unprecedentedly 40 Hz with over 250,000 measurement points per frame. Fig. 12 shows an example 3D frame that instantaneously displayed on a computer screen at 40 Hz.

Following this endeavor, numerous real-time techniques including [78–81] have been developed for 3D shape measurement leveraging both advanced hardware technologies (e.g., GPU) and new innovations on software algorithms.

As 3D shape measurement technologies become more accurate and faster, the number of potential applications in the field continue to grow including the medical field [82], the entertainment field (e.g., the creation of House of Card by Rockband Radiohead), and the manufacturing field.

3.4. Binary defocusing

By properly defocusing the projector, square binary patterns becomes pseudo sinusoidal patterns [83]. The DLP platforms (e.g., DLP Discovery, DLP LightCommander, and the DLP LightCrafter) can naturally display binary images at much faster rate (e.g., kHz) but they can

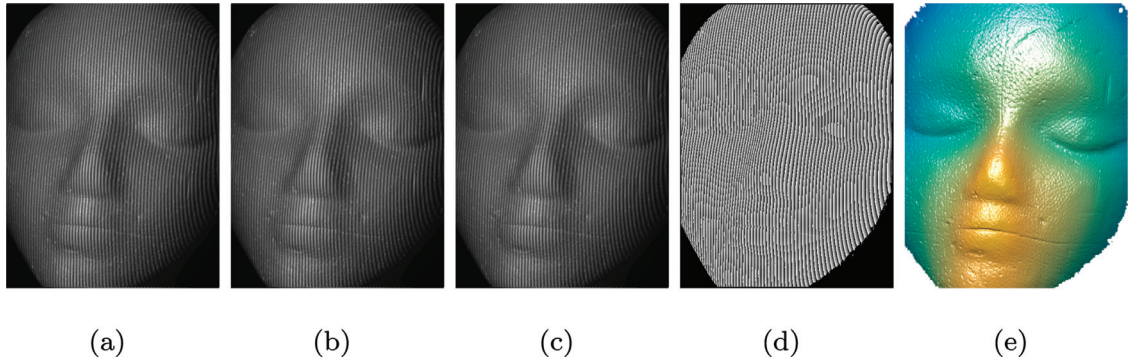


Fig. 11. 3D shape measurement using three-step phase shifting method. (a)-(c) Three phase-shifted fringe patterns; (d) wrapped phase; (e) recovered 3D shape.



Fig. 12. Simultaneous 3D shape acquisition, reconstruction, and display at 40 Hz. The right half image shows the subject being captured and the left image shows the reconstructed 3D geometry.

only display 8-bit grayscale images at a few hundred Hz. Therefore, if only binary images are necessary, 3D shape measurement rate can go up to kHz. As such, the digital binary defocusing technique [84] was developed.

Fig. 13 illustrates the concept of binary defocusing methods. Fig. 13a shows the square binary pattern and Fig. 13e shows the cross section of the pattern. When a Gaussian filter is applied to emulate the defocusing effect, the binary structures become less obvious as shown in Fig. 13b and e. Fig. 13c and g show the pattern appears sinusoidal when a certain size Gaussian filter is applied. However, if the filter size is too large, the contrast of the pattern decreases and the SNR reduces accordingly, as shown in Fig. 13d and g.

It has been demonstrated that using 1-bit binary patterns is advantageous over 8-bit sinusoidal phase-shifted fringe patterns especially on the DLP projection platform. Comparing with the conventional fringe projection technique that uses 8-bit fringe patterns, the binary defocusing techniques on the DLP platform has several major advantageous features: (1) it enabled speed breakthroughs [85]; (2) it relaxed the precise timing requirement between the DLP projector and the camera [86]; (3) it is immune to the projector's nonlinear response [86]; and (4) it allows higher depth resolution [87]. However, the binary defocusing method requires careful adjustment of the projector's lens to be within a small out-of-focus range, limiting its depth measurement capability.

Fig. 14 shows some representative frames of measuring a live beating rabbit heart using the binary defocusing method. For this particular measurement, the heart beats at approximately 180 beats/min. Three phase-shifted binary patterns are captured at 2000 Hz, and the corre-

sponding 3D shape measurement speed is 667 Hz. The algorithms employed for 3D shape reconstruction was developed by Wang et al. [88].

To improve phase quality, Fujita et al. [89] and Yoshizawa and Fujita [90] implemented the pulse width modulation (PWM) technique through hardware; Ayubi et al. [91] developed the sinusoidal pulse width modulation (SPWM) technique; Wang and Zhang [92] developed the optimal pulse width modulation (OPWM) technique; and later Zuo et al. [93] developed the optimization strategies for the SPWM technique. All these techniques could improve phase quality when the fringe period is relative small but fails to produce high-quality phase if the fringe period is too large or too small [94]. One of the reasons is that all these optimization strategies are based on 1D signal, yet fringe patterns are 2D.

2D optimization methods were developed to improve phase quality. Lohry and Zhang [95] developed an area modulation technique to create triangular wave instead of square wave to alleviate the harmonic error; Xian and Su developed the area modulation technique [96] to generate high-quality sinusoidal patterns through the high-accuracy fabrication; Wang and Zhang [97] employed the dithering/halftoning techniques [98–101] developed in the printing field to generate high-quality fringe patterns through defocusing; and various researchers [102–109] have developed the optimized dithering techniques to further improve phase quality. However, all area modulation and dithering technique only works well for large fringe periods. In summary, the attempts to optimize the binary pattern itself have substantially improved measurement quality, yet they only work well for a limited range of fringe periods especially when a small number of phase-shifted fringe patterns are used.

Researchers also attempted to improve phase quality produced by binary patterns by taking advantage of the temporally acquired information. Ayubi et al. [110] took 8 binary bits of the sinusoidal pattern, projected and captured each bit pattern separately, and finally combined those a single image for fringe analysis. This concept is great but it requires the acquisition of 8 images for each sinusoidal fringe pattern, which is not desirable for high-speed applications. Zhu et al. [111] reduced the image to be 4 by optimizing binary dithered patterns; Silva et al. [112] proposed the colored PWM technique to reduce the number of images to be three; Zuo et al. [113] only used 2 binary patterns and employed the triangular pulse width modulation (TPWM) technique; and Wang et al. [114] developed optimization strategies that only require 2 binary patterns to represent a single pattern for high-quality phase generation for broad range of fringe periods.

The DFP techniques has the advantage of speed, accuracy, flexibility, yet they all use a silicon-based digital projection devices such as liquid crystal display (LCD) or DLP projectors. The silicon based projection devices can only operate properly within a limited spectrum light range and a certain level light power. For example, the DLP projection system uses the silicon-based digital micro-mirror device (DMD), if the wavelength of light is over 2700 nm or below 300 nm, the transmission rate drops significantly [115]. In the meantime, the binary defocusing

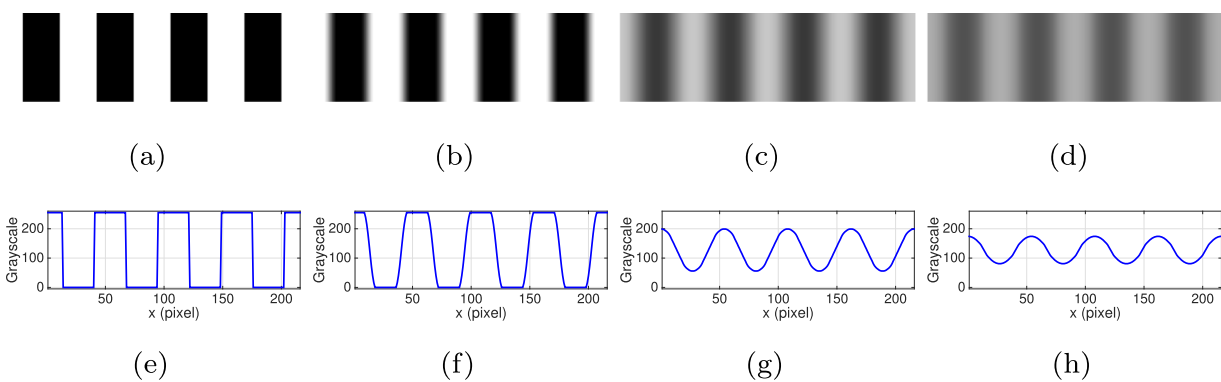


Fig. 13. Square binary pattern becomes pseudo sinusoidal pattern when a proper size Gaussian filter is applied. (a)–(d) The resultant binary pattern with increased filter sizes; (e)–(h) the corresponding cross sections.

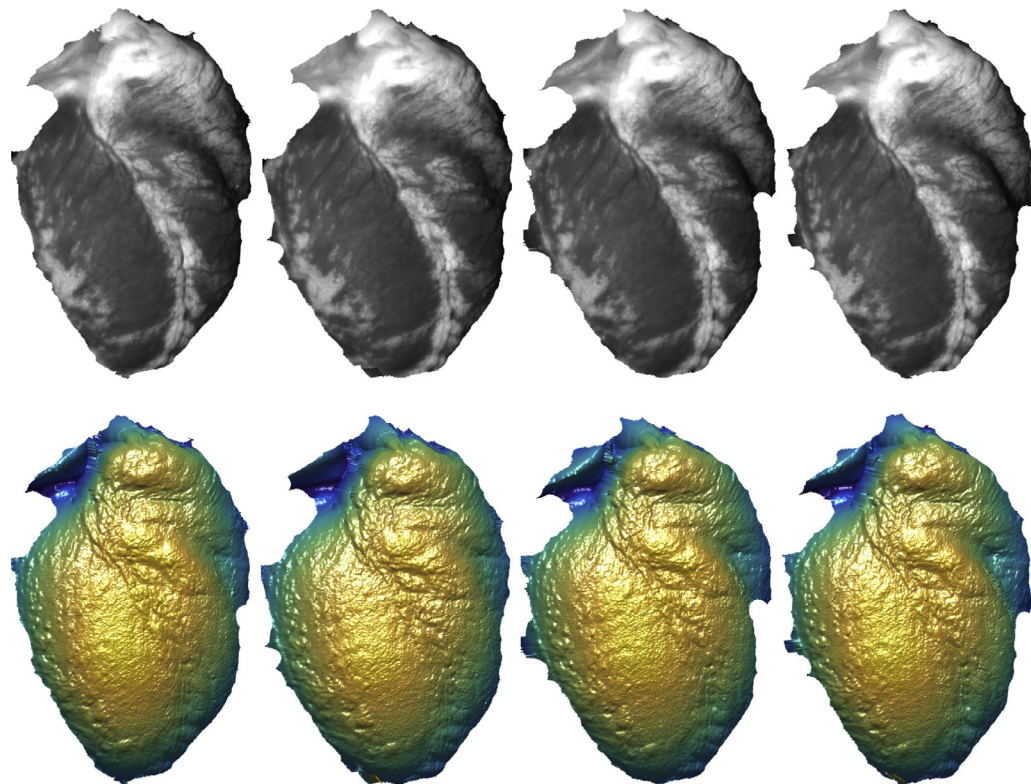


Fig. 14. Superfast 3D shape measurement of a live rabbit heart using the binary defocusing method. The first row shows texture images of 4 representative frames and the second row shows corresponding 3D reconstructions.

technique allows the use of binary patterns for high-quality 3D shape measurement, the precise grayscale values generated by digital video projectors is no longer necessary.

To overcome the spectrum limitation of DFP techniques and leverage the binary defocusing technique, Heist et al. [116] developed a system using two cameras and one mechanical projector with a rotating wheel. The rotating wheel has open and close slots to represent ON/OFF (i.e., binary) of the light. By properly defocusing lens, aperiodic sinusoidal patterns can be generated on the object surface. Since the projector does not use the silicon-based device for pattern generation, the light spectrum of the GOBO projector can be substantially broadened for applications such as 3D thermal imaging [117]. Even though high speed data acquisition (i.e., 1300 Hz) was realized, such a method did not precisely synchronize the projector with the camera and thus precise phase shifts cannot be ensured. Hyun et al. [118] developed a system that allows precise synchronization between the projector and the cam-

era, and employs a transparent film with locally unique statistical patterns to employ the improved computational framework developed by Lohry et al. [67]. The technique developed by Hyun et al. [118] can achieve 10,000 Hz 3D shape measurement speeds regardless the number of phase-shifted fringe patterns required for one 3D reconstruction. In contrast, if the DLP projection device is used, the 3D shape measurement rate is reduced if more number of phase-shifted fringe patterns are required.

Fig. 15 shows the photograph of the 3D shape measurement system using the mechanical projector. The system consists of two high-speed cameras and one mechanical projector that is an optical chopper. The timing generator takes the signal from the projector and sends precisely synchronized external signals to the cameras to capture images simultaneously. A statistical pattern on a transparent film was positioned immediately behind the projector to simplify correspondence determination. **Fig. 16** shows one example measurement. The measurement quality is

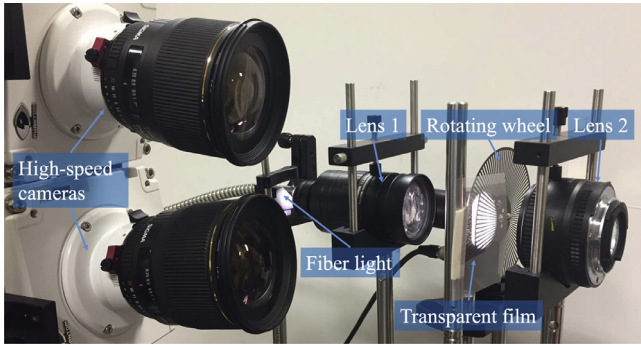


Fig. 15. Photograph of experimental system using a mechanical projector.

pretty high even when a three-step phase-shifting algorithm was used for phase computation.

Heist et al. [119] used LED array to create binary patterns for high-speed 3D shape measurement. Since LED can turn ON/OFF at extremely high rate (e.g., 100,000 Hz), 3D shape measurement speed can potentially be very high. Heist et al. [119] achieved a speed of approximately 330 Hz for a binary fringe projection rate of 3000 Hz. This technique, similar to the DLP based technique, the measurement speed is affected by the number of phase-shifted fringe patterns required for one 3D reconstruction.

3.5. Other coding methods

There are numerous other codification strategies developed for high-speed applications. For example, Garrihill and Hummel [120] developed the intensity ratio method, Jia et al. [121] developed the triangular phase-shifting method, and Huang et al. [122] the trapezoidal phase-shifting method. Color coded structured patterns [112,123,124] were also developed to reduce the number of required patterns and thus increase data acquisition speed. However, the methods of using color are typically sensitive to object surface color, making them difficult for an application where the scene is colorful.

Hybrid methods also developed primarily to enhance temporal phase unwrapping (e.g., improve robustness and/or speed). For instance, methods using phase-shifted pattern with embedded markers [125–132], a single stair pattern [133], ternary coded patterns [134], phase coded patterns [58,123,135–138], along with others.

4. Challenges

Despite drastic advancements in high-speed 3D shape measurement field including tremendous commercial successes, challenges remain to make advanced 3D shape measurement techniques accessible and available to solve challenging problems in science, engineering, industry, and our daily lives. This section lists some of the challenging problems that

worth exploring to further advance high-speed 3D shape measurement field.

4.1. Data storage

Nowadays, acquiring high-resolution and high-quality 3D range data in real time becomes increasingly convenient [139] propelled by the availability of commercial 3D sensors (e.g., Microsoft Kinect, iPhone X). However, there is one fundamental issue that has not been fully addressed: how can one effectively store and deliver such enormously large 3D data? Conventional 3D geometry representation methods including OBJ, PLY, and STL can represent arbitrary 3D geometry and texture data, but the file size is enormous (typically at least one order of magnitude larger than 2D counter parts). Efforts [140–151] have been made to compress 3D range data, yet none of the state-of-the-art methods is ubiquitous for efficient 3D data storage.

4.2. Sensor miniaturization

High-speed 3D shape measurement methods using a single statistical pattern based methods have seen great success in miniaturization. For example, Apple iPhone X employed the statistical pattern method for face ID and virtual reality (VR) applications on high-end smart phones, and Intel RealSense attempted to miniaturize the binary coding method for human computer interaction (HCI) applications. However, neither resolution nor accuracy achieved on these devices is comparable to that achieved by advanced structured light methods. Efforts on miniaturizing accurate 3D sensing technologies is highly needed to increase their application areas.

4.3. Tough object measurement

All structured light methods are based on optics, and thus such methods face challenges if an object surface is not optical friendly (e.g., shiny parts). Researchers have developed various techniques to handle shiny, transparent, or high dynamic range parts [152–171], yet none of such techniques is mature enough to measure arbitrary objects rapidly and accurately without human intervention. Furthermore, although structured light technologies have been employed in various applications, the consistency and repeatability of high-speed 3D shape measurement techniques are often difficult to ensure especially when commercially available hardware components are used. For example, when a standard digital video projector is used for 3D shape measurement, the thermal and noise impact could significantly influence measurement accuracy.

4.4. Automation

Historically, 2D imaging technologies evolved from when only professional photographers can take good pictures to nowadays that a 2-year old kid can do it with a smart phone. The major breakthroughs occurred between 1950s–1980s that led to easy-to-use 2D cameras that

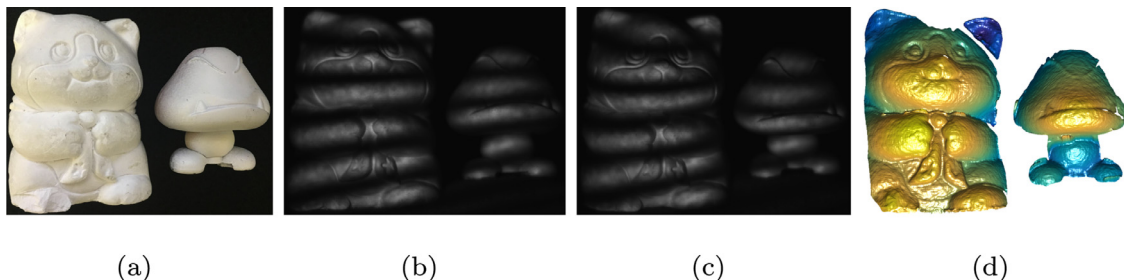


Fig. 16. 3D shape measurement using the mechanical projection system. (a) Photograph of the object; (b) one of the phase shifted fringe patterns from the left camera; (c) one of the phase shifted fringe patterns from the right camera; (d) recovered 3D shape.

eventually become the 2D camera technologies today. One of the key innovations towards the easy to use 2D imaging technologies is the automation that allows the camera to be easily setup and used by a consumer without expert knowledge on imaging processing. Unfortunately, comparing with the relatively mature high-quality 2D imaging technologies, 3D counterparts are still in their infancy. The current high-accuracy 3D optical metrology technology on the market are, to a great extent, very similar to those 2D technologies before 1900s when 35 mm cameras were not invented. The limited study [172] thus far on automatic necessitates the better automated methods to make 3D shape measurement technologies ubiquitously accessible.

4.5. Applications

Though numerous robust 3D shape measurement techniques have been developed, none of the existing techniques can solve all application problems with some applications being more challenging than others. Furthermore, even though some existing techniques could solve an application problem, the approach may not be optimized in terms of cost, efficiency, simplicity, or robustness. For each application, the technology has to be optimized, to various degrees, to achieve best performance. Yet, it still lacks of the tools that can perform such optimization easily and rapidly for non-experts.

5. Summary

This paper has presented the state-of-the-art 3D shape measurement techniques based on structured light methods, especially those techniques that could achieve high measurement speed and accuracy. We explained the basic principles with each technology, demonstrated the capabilities/limitations of some popular 3D shape measurement techniques through experimental data, and casted our perspectives on some challenges to be overcome to make advanced 3D shape measurement techniques ubiquitous.

Acknowledgments

The author would like to thank my current and former collaborators, students, and researchers who made high-speed 3D shape measurement an exciting and enriching fields. In particular, the authors would like to thank his current and former students Jae-sang Hyun, Chufan Jiang, Beiwen Li, Ziping Liu, and Yajun Wang for their help in generating data for this paper, and Professor Igor R. Efimov and Dr. Kedar Aras from George Washington University for the heart experiments. Last but not the least, the author would like to thank Professor Kemao Qian for his invitation to contribute to this special issue.

This work were supported by National Science Foundation under grant numbers (CMMI-1531048, CMMI-1523048, and NRI-1637961).

Supplementary material

Supplementary material associated with this article can be found, in the online version, at doi:10.1016/j.optlaseng.2018.02.017.

References

- [1] Dhond UR, Aggarwal JK. Structure from stereo-a review. *IEEE Trans Syst Man Cybern* 1989;19(6):1489–510.
- [2] Lazaros N, Sirakoulis GC, Gasteratos A. Review of stereo vision algorithms: from software to hardware. *Int J Optomechatron* 2008;2(4):435–62.
- [3] Hansard M, Lee S, Choi O, Horaud RP. Time-of-Flight cameras. Springer-Verlag London; 2013.
- [4] Salvi J, Fernandez S, Pribanic T, Llado X. A state of the art in structured light patterns for surface profilometry. *Patt Recogn* 2010;43(8):2666–80.
- [5] Zhang S. Recent progresses on real-time 3-d shape measurement using digital fringe projection techniques. *Opt Laser Eng* 2010;48(2):149–58.
- [6] der Jeught SV, Dirckx JJ. Real-time structured light profilometry: a review. *Opt Laser Eng* 2016;87:18–31.
- [7] Zhang Z. Review of single-shot 3d shape measurement by phase calculation-based fringe projection techniques. *Opt Laser Eng* 2012;50(8):1097–106.
- [8] Takeda M. Fourier fringe analysis and its applications to metrology of extreme physical phenomena: a review. *Appl Opt* 2013;52(1):20–9.
- [9] Su X, Zhang Q. Dynamic 3-d shape measurement method: a review. *Opt Laser Eng* 2010;48:191–204.
- [10] Geng J. Structured-light 3d surface imaging: a tutorial. *Adv Opt Photon* 2011;3(2):128–60.
- [11] Scharstein D, Szeliski R. A taxonomy and evaluation of dense two-frame stereo correspondence algorithms. *Intl J Comp Vis* 2002;47(1–3):7–42.
- [12] Hartley RI, Zisserman A. Multiple view geometry in computer vision. Cambridge University Press; 2000. ISBN: 0521623049.
- [13] Kolmogorov V, Zabih R. Multi-camera scene reconstruction via graph cuts. In: Proceedings of the European Conference on Computer Vision; 2002. p. 82–96.
- [14] Kostková J, Sára R. Stratified dense matching for stereopsis in complex scenes.. In: Proceedings of the British Machine Vision Conference; 2003. p. 339–48.
- [15] Hirschmuller H. Stereo processing by semiglobal matching and mutual information. *IEEE Trans Pattern Anal Mach Intell* 2008;30(2):328–41.
- [16] Besse F, Rother C, Fitzgibbon AW, Kautz J. PMBP: patchmatch belief propagation for correspondence field estimation. *Intl J Comp Vis* 2013;110(1):2–13.
- [17] Xu S, Zhang F, He X, Shen X, Zhang X. Pm-pm: patchmatch with potts model for object segmentation and stereo matching. *IEEE Trans Image Proc* 2015;24(7):2182–96.
- [18] Zhu S, Yan L. Local stereo matching algorithm with efficient matching cost and adaptive guided image filter. *Vis Comput* 2017;33(9):1087–102.
- [19] Kanade T, Okutomi M. A stereo matching algorithm with an adaptive window: theory and experiment. *IEEE Trans Pattern Anal Mach Intell* 1994;16(9):920–32.
- [20] Li B, An Y, Cappelleri D, Xu J, Zhang S. High-accuracy, high-speed 3d structured light imaging techniques and potential applications to intelligent robotics. *Int J Intel Robot Appl* 2017;1(1):86–103.
- [21] Wen Y, Li S, Cheng H, Su X, Zhang Q. Universal calculation formula and calibration method in fourier transform profilometry. *Appl Opt* 2010;49(34):6563–9.
- [22] Xiao Y, Cao Y, Wu Y. Improved algorithm for phase-to-height mapping in phase measuring profilometry. *Appl Opt* 2012;51(8):1149–55.
- [23] Villa Y, Araiza M, Alaniz D, Ivanov R, Ortiz M. Transformation of phase to (x,y,z)-coordinates for the calibration of a fringe projection profilometer. *Opt Laser Eng* 2012;50(2):256–61.
- [24] Xu Y, Ekstrand L, Dai J, Zhang S. Phase error compensation for three-dimensional shape measurement with projector defocusing. *Appl Opt* 2011;50(17):2572–81.
- [25] Zhang Z. A flexible new technique for camera calibration. *IEEE Trans Pattern Anal Mach Intell* 2000;22(11):1330–4.
- [26] Duane CB. Close-range camera calibration. *Photogram Eng* 1971;37(8):855–66.
- [27] Sobel I. On calibrating computer controlled cameras for perceiving 3-d scenes. *Artif Intell* 1974;5(2):185–98.
- [28] Tsai R. A versatile camera calibration technique for high-accuracy 3d machine vision metrology using off-the-shelf tv cameras and lenses. *IEEE J Robot Autom* 1987;3(4):323–44.
- [29] Hu Q, Huang PS, Fu Q, Chiang F-P. Calibration of a three-dimensional shape measurement system. *Opt Eng* 2003;42(2):487–93.
- [30] Mao X, Chen W, Su X. Improved fourier-transform profilometry. *Appl Opt* 2007;46(5):664–8.
- [31] Zappa E, et al. Fourier-transform profilometry calibration based on an exhaustive geometric model of the system. *Opt Laser Eng* 2009;47(7):754–67.
- [32] Guo H, Chen M, Zheng P. Least-squares fitting of carrier phase distribution by using a rational function in fringe projection profilometry. *Opt Lett* 2006;31(24):3588–90.
- [33] Du H, Wang Z. Three-dimensional shape measurement with an arbitrarily arranged fringe projection profilometry system. *Opt Lett* 2007;32(16):2438–40.
- [34] Huang L, Chua PS, Asundi A. Least-squares calibration method for fringe projection profilometry considering camera lens distortion. *Appl Opt* 2010;49(9):1539–48.
- [35] Vo M, Wang Z, Pan B, Pan T. Hyper-accurate flexible calibration technique for fringe-projection-based three-dimensional imaging. *Opt Express* 2012;20(15):16926–41.
- [36] Zhang S, Huang PS. Novel method for structured light system calibration. *Opt Eng* 2006;45(8):083601.
- [37] Li B, Karpinsky N, Zhang S. Novel calibration method for structured light system with an out-of-focus projector. *Appl Opt* 2014;53(13):3415–26.
- [38] Bell T, Zhang S. Method for out-of-focus camera calibration. *Appl Opt* 2016;55(9):2346–52.
- [39] An Y, Bell T, Li B, Xu J, Zhang S. Novel method for large range structured light system calibration. *Appl Opt* 2016;55(33):9563–72.
- [40] Rusinkiewicz S, Hall-Holt O, Levoy M. Real-time 3d model acquisition. *ACM Trans Graph* 2002;21(3):438–46.
- [41] Hall-Holt O, Rusinkiewicz S. Stripe boundary codes for real-time structured-light range scanning of moving objects. In: Proceedings of the 8th IEEE International Conference on Computer Vision; 2001 II:359–366.
- [42] Davis J, Ramamoorthi R, Rusinkiewicz S. Spacetime stereo: a unifying framework for depth from triangulation. In: Proceedings of the IEEE Conference on Computer Vision and Pattern Recognition, 2; 2003 II:359–66 vol.2.
- [43] Zhang L, Curless B, Seitz S. Spacetime stereo: shape recovery for dynamic scenes. In: Proceedings of the Computer Vision and Pattern Recognition; 2003. p. 367–74.
- [44] Zhang L, Snavely N, Curless B, Seitz SM. Spacetime faces: high-resolution capture for modeling and animation. *ACM Trans Graph* 2004;23(3):548–58.
- [45] Grigull V, Rottenkolber H. Two beam interferometer using a laser. *J Opt Soc Am* 1967;57(2):149–55.
- [46] Schmit J, Creath K, Wyant JC. Surface profilers, multiple wavelength, and white light interferometry. 3rd. John Wiley & Sons; 2007. p. 667–755.

- [47] Anderson JA, Porter RW. Ronchi'S method of optical tesing. *Astrophys J* 1929;70:175–81.
- [48] Rowe SH, Welford WT. Surface topography of non-optical surfaces by projected interference fringes. *Nature* 1967;216(5117):786–7.
- [49] Takeda M, Mutoh K. Fourier transform profilometry for the automatic measurement of 3-d object shapes. *Appl Opt* 1983;22:3977–82.
- [50] Ghiglia DC, Pritt MD editors. Two-dimensional phase unwrapping: theory, algorithms, and software. New York: John Wiley and Sons; 1998.
- [51] Su X, Chen W. Reliability-guided phase unwrapping algorithm: a review. *Opt Laser Eng* 2004;42(3):245–61.
- [52] Cheng Y-Y, Wyant JC. Two-wavelength phase shifting interferometry. *Appl Opt* 1984;23:4539–43.
- [53] Cheng Y-Y, Wyant JC. Multiple-wavelength phase shifting interferometry. *Appl Opt* 1985;24:804–7.
- [54] Towers DP, Jones JDC, Towers CE. Optimum frequency selection in multi-frequency interferometry. *Opt Lett* 2003;28:1–3.
- [55] Wang Y, Zhang S. Superfast multifrequency phase-shifting technique with optimal pulse width modulation. *Opt Express* 2011;19(6):5143–8.
- [56] Sansoni G, Caroccia M, Rodella R. Three-dimensional vision based on a combination of gray-code and phase-shift light projection: analysis and compensation of the systematic errors. *Appl Opt* 1999;38:6565–73.
- [57] Zhang S. Flexible 3d shape measurement using projector defocusing: extended measurement range. *Opt Lett* 2010;35(7):931–3.
- [58] Wang Y, Zhang S. Novel phase coding method for absolute phase retrieval. *Opt Lett* 2012;37(11):2067–9.
- [59] Zuo C, Chen Q, Gu G, Feng S, Feng F, Li R, et al. High-speed three-dimensional shape measurement for dynamic scenes using bi-frequency tripolar pulse-width-modulation fringe projection. *Opt Lasers Eng* 2013;51(8):953–60.
- [60] Xing Y, Quan C, Tay C. A modified phase-coding method for absolute phase retrieval. *Opt Lasers Eng* 2016;87:97–102.
- [61] Zuo C, Huan L, Zhang M, Chen Q, Asundi A. Temporal phase unwrapping algorithms for fringe projection profilometry: a comparative review. *Opt Laser Eng* 2016;85:84–103.
- [62] An Y, Hyun J-S, Zhang S. Pixel-wise absolute phase unwrapping using geometric constraints of structured light system. *Opt Express* 2016;24(15):18445–59.
- [63] Zhong K, Li Z, Shi Y, Wang C, Lei Y. Fast phase measurement profilometry for arbitrary shape objects without phase unwrapping. *Opt Lasers Eng* 2013;51(11):1213–22.
- [64] Li Z, Zhong K, Li YF, Zhou X, Shi Y. Multiview phase shifting: a full-resolution and high-speed 3d measurement framework for arbitrary shape dynamic objects. *Opt Lett* 2013;38(9):1389–91.
- [65] Bräuer-Burchardt C, Kühmstedt P., Notni G. Code minimization for fringe projection based 3d stereo sensors by calibration improvement. Technical report2014. arXiv:1404.7298.
- [66] Song K, Hu S, Wen X, Yan Y. Fast 3d shape measurement using fourier transform profilometry without phase unwrapping. *Opt Lasers Eng* 2016;84:74–81.
- [67] Lohry W, Chen V, Zhang S. Absolute three-dimensional shape measurement using coded fringe patterns without phase unwrapping or projector calibration. *Opt Express* 2014;22(2):1287–301.
- [68] Kema Q. Windowed fourier transform for fringe pattern analysis. *Appl Opt* 2004;43:2695–702.
- [69] Kema Q. Two-dimensional windowed fourier transform for fringe pattern analysis: principles, applications and implementations. *Opt Laser Eng* 2007;45:304–17.
- [70] Qian K. Comparison of fourier transform, windowed fourier transform, and wavelet transform methods for phase extraction from a single fringe pattern in fringe projection profilometry. *Opt Laser Eng* 2010;48(2):141–8.
- [71] Qian K. Applications of windowed fourier fringe analysis in optical measurement: a review. *Opt Laser Eng* 2015;66:67–73.
- [72] Guo L, Su X, Li J. Improved fourier transform profilometry for the automatic measurement of 3d object shapes. *Opt Eng* 1990;29(12):1439–44.
- [73] Guo H, Huang PS. Absolute phase technique for the fourier transform method. *Opt Eng* 2009;48(4):043609.
- [74] Zhang Q, Su X. High-speed optical measurement for the drumhead vibration. *Opt Express* 2005;13(8):3110–16.
- [75] Li B, Zhang S. Superfast, high-resolution absolute 3d recovery of a stabilized flapping flight process. *Opt Express* 2017;25(22):27270–82.
- [76] Malacara D. Optical shop testing. 3rd. New York, NY: John Wiley and Sons; 2007.
- [77] Zhang S, Huang PS. High-resolution real-time three-dimensional shape measurement. *Opt Eng* 2006;45(12):123601.
- [78] Zhang S, Royer D, Yau S-T. Gpu-assisted high-resolution, real-time 3-d shape measurement. *Opt Express* 2006;14(20):9120–9.
- [79] Liu K, Wang Y, Lau DL, Hao Q, Hassebrook LG. Dual-frequency pattern scheme for high-speed 3-d shape measurement. *Opt Express* 2010;18:5229–44.
- [80] Jones A, Lang M, Fyffe G, Yu X, Busch J, McDowall I, et al. Achieving eye contact in a one-to-many 3d video teleconferencing system. *ACM Trans Graph* 2009;28(3):64:1–64:8.
- [81] Weise T, Leibe B, Gool LV. Fast 3d scanning with automatic motion compensation. In: Proceedings of the IEEE Conference on Computer Vision and Pattern Recognition (CVPR); 2007. p. 1–8.
- [82] Mehta RP, Zhang S, Hadlock TA. Novel 3-d video for quantification of facial movement. *Otolaryngol Head Neck Surg* 2008;138(4):468–72.
- [83] Su XY, Zhou WS, Von Balla G, Vukicevic D. Automated phase-measuring profilometry using defocused projection of a ronchi grating. *Opt Commun* 1992;94:561–73.
- [84] Lei S, Zhang S. Flexible 3-d shape measurement using projector defocusing. *Opt Lett* 2009;34(20):3080–2.
- [85] Zhang S, van der Weide D, Oliver J. Superfast phase-shifting method for 3-d shape measurement. *Opt Express* 2010;18(9):9684–9.
- [86] Lei S, Zhang S. Digital sinusoidal fringe generation: defocusing binary patterns vs focusing sinusoidal patterns. *Opt Laser Eng* 2010;48(5):561–9.
- [87] Li B, Zhang S. Microscopic structured light 3d profilometry: binary defocusing technique vs sinusoidal fringe projection. *Opt Laser Eng* 2017;96:117–23.
- [88] Wang Y, Laughner JI, Efimov IR, Zhang S. 3D absolute shape measurement of live rabbit hearts with a superfast two-frequency phase-shifting technique. *Opt Express* 2013;21(5):5822–5632.
- [89] Fujita H, Yamatan K, Yamamoto M, Otani Y, Suguro A, Morokawa S, et al. Three-dimensional profilometry using liquid crystal grating. In: Proceedings of the SPIE, Beijing, China, 5058; 2003. p. 51–60.
- [90] Yoshizawa T, Fujita H. Liquid crystal grating for profilometry using structured light. In: Proceedings of the SPIE, Boston, MA, 6000; 2005. p. 60000H1–10.
- [91] Ayubi GA, Ayubi JA, Martino JMD, Ferrari JA. Pulse-width modulation in defocused 3-d fringe projection. *Opt Lett* 2010;35:3682–4.
- [92] Wang Y, Zhang S. Optimal pulse width modulation for sinusoidal fringe generation with projector defocusing. *Opt Lett* 2010;35(24):4121–3.
- [93] Zuo C, Chen Q, Feng S, Feng F, Gu G, Sui X. Optimized pulse width modulation pattern strategy for three-dimensional profilometry with projector defocusing. *Appl Opt* 2012;51(19):4477–90.
- [94] Wang Y, Zhang S. Comparison among square binary, sinusoidal pulse width modulation, and optimal pulse width modulation methods for three-dimensional shape measurement. *Appl Opt* 2012;51(7):861–72.
- [95] Lohry W, Zhang S. 3D shape measurement with 2d area modulated binary patterns. *Opt Laser Eng* 2012;50(7):917–21.
- [96] Xian T, Su X. Area modulation grating for sinusoidal structure illumination on phase-measuring profilometry. *Appl Opt* 2001;40(8):1201–6.
- [97] Wang Y, Zhang S. Three-dimensional shape measurement with binary dithered patterns. *Appl Opt* 2012;51(27):6631–6.
- [98] Bayer B. An optimum method for two-level rendition of continuous-tone pictures. *IEEE Int Conf Commun* 1973;1:11–15.
- [99] Kite TD, Evans BL, Bovik AC. Modeling and quality assessment of halftoning by error diffusion. In: Proceedings of the IEEE International Conference on Image Processing, 9; 2000. p. 909–22.
- [100] Floyd R, Steinberg L. An adaptive algorithm for spatial gray scale. In: Proceedings of the Society for Information Display, 17; 1976. p. 75–7.
- [101] Stucki P, Mecca multiple-error correcting computation algorithm for bilevel hard-copy reproduction. Technical Report. Zurich, Switzerland: IBM Res. Lab.; 1981.
- [102] Lohry W, Zhang S. Genetic method to optimize binary dithering technique for high-quality fringe generation. *Opt Lett* 2013;38(4):540–2.
- [103] Dai J, Li B, Zhang S. Intensity-optimized dithering technique for high-quality 3d shape measurement. *Opt Laser Eng* 2014;53:79–85.
- [104] Dai J, Zhang S. Phase-optimized dithering technique for high-quality 3d shape measurement. *Opt Laser Eng* 2013;51(6):790–5.
- [105] Dai J, Li B, Zhang S. High-quality fringe patterns generation using binary pattern optimization through symmetry and periodicity. *Opt Laser Eng* 2014;52:195–200.
- [106] Sun J, Zuo C, Feng S, Yu S, Zhang Y, Chen Q. Improved intensity-optimized dithering technique for 3d shape measurement. *Opt Laser Eng* 2015;66:158–64.
- [107] Xiao Y, Li Y. High-quality binary fringe generation via joint optimization on intensity and phase. *Opt Laser Eng* 2017;97:19–26.
- [108] Li X-X, Zhang Z-J. High-quality fringe pattern generation based on binary pattern optimization with projector defocusing. *J Opt Technol* 2017;84(1):22–8.
- [109] Tian Z, Chen W, Su X. Method for improving sinusoidal quality of error diffusion binary encoded fringe used in phase measurement profilometry. *Optica Applicata* 2016;46(2):291–303.
- [110] Ajubi GA, Ayubi JA, Martino JMD, Ferrari JA. Three-dimensional profiling with binary fringes using phase-shifting interferometry algorithms. *Appl Opt* 2011;50(2):147–54.
- [111] Zhu J, Zhou P, Su X, You Z. Accurate and fast 3d surface measurement with temporal-spatial binary encoding structured illumination. *Opt Express* 2016;24(25):28549–60.
- [112] Silva A, Flores JL, Munoz A, Ayubi GA, Ferrari JA. Three-dimensional shape profiling by out-of-focus projection of colored pulse width modulation fringe patterns. *Appl Opt* 2017;56(18):5198–203.
- [113] Zuo C, Chen Q, Gu G, Feng S, Feng F, Li R, et al. High-speed three-dimensional shape measurement for dynamic scenes using bi-frequency tripolar pulse-width-modulation fringe projection. *Opt Laser Eng* 2013;51(8):953–60.
- [114] Wang Y, Jiang C, Zhang S. Double-pattern triangular pulse width modulation technique for high-accuracy high-speed 3d shape measurement. *Opt Express* 2017;25(24):30177–88.
- [115] Dudley D, Duncan W, Slaughter J. Emerging digital micromirror device (dmd) applications. In: Proceedings of the SPIE, 4985; 2003. p. 1.
- [116] Heist S, Lutzke P, Schmidt I, Dietrich P, Kühmstedt P, Tünnermann A, et al. High-speed three-dimensional shape measurement using gobo projection. *Opt Laser Eng* 2016;87:90–6.
- [117] Brahm A, Rößler C, Dietrich P, Heist S, Kühmstedt P, Notni G. Non-destructive 3d shape measurement of transparent and black objects with thermal fringes. In: Proceedings of the SPIE, 9868; 2016. p. 98680C.
- [118] Hyun J-S, Chiu GT-C, Zhang S. High-speed and high-accuracy 3d surface measurement using a mechanical projector. *Opt Express* 2018;26(2):1474–87.
- [119] Heist S, Mann A, Kühmstedt P, Schreiber P, Notni G. Array projection of aperiodic sinusoidal fringes for high-speed three-dimensional shape measurement. *Opt Eng* 2014;53(11):112208.
- [120] Carrillib R, Hummel R. Experiments with the intensity ratio depth sensor. *Comput Vis Graph Image Process* 1985;32:337–58.

- [121] Jia P, Kofman J, English C. Two-step triangular-pattern phase-shifting method for three-dimensional object-shape measurement. *Opt Eng* 2007;46(8):083201.
- [122] Huang PS, Zhang S, Chiang F-P. Trapezoidal phase-shifting method for three-dimensional shape measurement. *Opt Eng* 2005;44(12):123601.
- [123] Chen X, Lu C, Ma M, Mao X, Mei T. Color-coding and phase-shift method for absolute phase measurement. *Opt Comm* 2013;298:54–8.
- [124] Pan J, Huang PS, Chiang F-P. Color phase-shifting technique for three-dimensional shape measurement. *Opt Eng* 2006;45(12):013602.
- [125] Cruz-Santos W, Lopez-Garcia L. Implicit absolute phase retrieval in digital fringe projection without reference lines. *Appl Opt* 2015;54(7):1688–95.
- [126] Guo H, Huang P. 3-d shape measurement by use of a modified fourier transform method. In: Proceedings of the SPIE, 7066; 2008. p. 70660E.
- [127] Zhang S, Yau S-T. High-resolution, real-time 3-d absolute coordinate measurement based on a phase-shifting method. *Opt Express* 2006;14(7):2644–9.
- [128] Su X, Zhang Q, Xiao Y, Xiang L. Dynamic 3-d shape measurement techniques with marked fringes tracking. In: Proceedings of the Fringe 2009; 2009. p. 493–6.
- [129] Cui H, Liao W, Dai N, Cheng X. A flexible phase-shifting method with absolute phase marker retrieval. *Measurement* 2012;45(1):101–8.
- [130] Xiao Y, Su X, Zhang Q, Li Z. 3-D profilometry for the impact process with marked fringes tracking. *Opto-Electron Eng* 2007;34(8):46–52.
- [131] Budianto B, Lun P, Hsung T-C. Marker encoded fringe projection profilometry for efficient 3d model acquisition. *Appl Opt* 2014;53(31):7442–53.
- [132] Cong P, Xiong Z, Zhang Y, Zhao S, Wu F. Accurate dynamic 3d sensing with fourier-assisted phase shifting. *IEEE J Sel Top Signal Process* 2015;9(3):396–408.
- [133] Zhang S. Composite phase-shifting algorithm for absolute phase measurement. *Opt Laser Eng* 2012;50(11):1538–41.
- [134] Zheng D, Kemao Q, Da F, Seah HS. Ternary gray code-based phase unwrapping for 3d measurement using binary patterns with projector defocusing. *Appl Opt* 2017;56(13):3660–5.
- [135] Zhou C, Liu T, Si S, Xu J, Liu Y, Lei Z. Phase coding method for absolute phase retrieval with a large number of codewords. *Opt Express* 2012;20(22):24139–50.
- [136] Zhou C, Liu T, Si S, Xu J, Liu Y, Lei Z. An improved stair phase encoding method for absolute phase retrieval. *Opt Laser Eng* 2015;66:269–78.
- [137] Xing Y, Quan C, Tay C. A modified phase-coding method for absolute phase retrieval. *Opt Laser Eng* 2016;87:97–102.
- [138] Hyun J, Zhang S. Superfast 3d absolute shape measurement using five fringe patterns. *Opt Laser Eng* 2017;90:217–24.
- [139] Zhang S. High-speed 3D imaging with digital fringe projection technique. 1st. New York, NY: CRC Press; 2016.
- [140] Karpinsky N, Zhang S. Composite phase-shifting algorithm for three-dimensional shape compression. *Opt Eng* 2010;49(6):063604.
- [141] Karpinsky N, Zhang S. 3D range geometry video compression with the h.264 codec. *Opt Laser Eng* 2013;51(5):620–5.
- [142] Karpinsky N, Zhang S. Holovideo: real-time 3d video encoding and decoding on GPU. *Opt Laser Eng* 2012;50(2):280–6.
- [143] Wang Y, Zhang L, Yang S, Ji F. Two-channel high-accuracy hololimage technique for three-dimensional data compression. *Opt Laser Eng* 2016;85:48–52.
- [144] Hou Z, Su X, Zhang Q. Virtual structured-light coding for three-dimensional shape data compression. *Opt Laser Eng* 2012;50(6):844–9.
- [145] Zhang S. Three-dimensional range data compression using computer graphics rendering pipeline. *Appl Opt* 2012;51(18):4058–64.
- [146] Ou P, Zhang S. Natural method for three-dimensional range data compression. *Appl Opt* 2013;52(9):1857–63.
- [147] Bell T, Zhang S. Multi-wavelength depth encoding method for 3d range geometry compression. *Appl Opt* 2015;54(36):10684–961.
- [148] Karpinsky N, Wang Y, Zhang S. Three bit representation of three-dimensional range data. *Appl Opt* 2013;52(11):2286–93.
- [149] Peng J, Kim C-S, Kuo C-C J. Technologies for 3d mesh compression: a survey. *J Vis Commun Image Represent* 2005;16(6):688–733.
- [150] Alliez P, Gotsman C. Recent advances in compression of 3d meshes. Berlin, Heidelberg: Springer Berlin Heidelberg; 2005. p. 3–26.
- [151] Maglo A, Lavoué G, Dupont F, Hudelot C. 3D mesh compression: survey, comparisons, and emerging trends. *ACM Comput Surv* 2015;47(3):44:1–44:41.
- [152] Song Z, Jiang H, Lin H, Tang S. A high dynamic range structured light means for the 3d measurement of specular surfaces. *Opt Laser Eng* 2017;95:8–16.
- [153] Lin H, Gao J, Mei Q, Zhang G, He Y, Chen X. Three-dimensional shape measurement technique for shiny surfaces by adaptive pixel-wise projection intensity adjustment. *Opt Laser Eng* 2017;91:206–15.
- [154] Koutecký T, Paloušek D, Brandejs J. Sensor planning system for fringe projection scanning of sheet metal parts. *Measurement* 2016;94:60–70.
- [155] Feng S, Chen Q, Zuo C, Asundi A. Fast three-dimensional measurements for dynamic scenes with shiny surfaces. *Opt Comm* 2017;382:18–27.
- [156] Waddington C, Kofman J. Camera-independent saturation avoidance in measuring high-reflectivity-variation surfaces using pixel-wise composed images from projected patterns of different maximum gray level. *Opt Comm* 2014;333:32–7.
- [157] Babaie G, Abolbashari M, Farahi F. Dynamics range enhancement in digital fringe projection technique. *Precision Eng* 2015;39:243–51.
- [158] Wang M, Du G, Zhou C, Zhang C, Si S, Li H, et al. Enhanced high dynamic range 3d shape measurement based on generalized phase-shifting algorithm. *Opt Comm* 2014;385:43–53.
- [159] Lin H, Gao J, Mei Q, He Y, Liu J, Wang X. Adaptive digital fringe projection technique for high dynamic range three-dimensional shape measurement. *Opt Express* 2016;24:7703–18.
- [160] Feng S, Zhang Y, Chen Q, Zuo C, Li R, Shen G. General solution for high dynamic range three-dimensional shape measurement using the fringe projection technique. *Opt Laser Eng* 2014;59:56–71.
- [161] Li S, Da F, Rao L. Adaptive fringe projection technique for high-dynamic range three-dimensional shape measurement using binary search. *Opt Eng* 2017;56:094111.
- [162] Long Y, Wang S, Wu W, Liu K. Accurate identification of saturated pixels for high dynamic range measurement. *Opt Eng* 2015;54:043106.
- [163] Salahieh B, Chen Z, Rodriguez JJ, Liang R. Multi-polarization fringe projection imaging for high dynamic range objects. *Opt Express* 2014;22:10064–71.
- [164] Yamaguchi Y, Miyake H, Nishikawa O, Iyoda T. Shape measurement of glossy objects by range finder with polarization optical system. *Gazo Denshi Gakkai Kenkyukai Koen Yoko* (in Japanese) 2003;200:43–50.
- [165] Kokku R, Brooksby G. Improving 3d surface measurement accuracy on metallic surfaces. In: Proceedings of the SPIE, 5856; 2005. p. 618–24.
- [166] Hu Q, Harding KG, Du X, Hamilton D. Shiny parts measurement using color separation. In: Proceedings of the SPIE, 6000; 2005. p. 6000D1–8.
- [167] Waddington C, Kofman J. Analysis of measurement sensitivity to illuminance and fringe-pattern gray levels for fringe-pattern projection adaptive to ambient lighting. *Opt Laser Eng* 2010;48:251–6.
- [168] Jiang H, Zhao H, Li X. High dynamic range fringe acquisition: a novel 3-d scanning technique for high-reflective surfaces. *Opt Laser Eng* 2012;50:1484–93.
- [169] Zhao H, Liang X, Diao X, Jiang H. Rapid in-situ 3d measurement of shiny object based on fast and high dynamic range digital fringe projector. *Opt Laser Eng* 2014;54:170–4.
- [170] Jiang C, Bell T, Zhang S. High dynamic range real-time 3d shape measurement. *Opt Express* 2016;24(7):7337–46.
- [171] Chen B, Zhang S. High-quality 3d shape measurement using saturated fringe patterns. *Opt Laser Eng* 2016;87:83–9.
- [172] Ekstrand L, Zhang S. Auto-exposure for three-dimensional shape measurement with a digital-light-processing projector. *Opt Eng* 2011;50(12):123603.